

**ACTIVATED CARBON DERIVED FROM  
*PENTACE TRIPTERA*, *INTSIA BIJUGA* AND  
*HEVEA BRASILIENSIS* SAWDUST VIA  
MICROWAVE-INDUCED POTASSIUM  
HYDROXIDE ACTIVATION FOR DYES  
ADSORPTION**

by

**AZDUWIN BINTI KHASRI**

**Thesis submitted in fulfilment of the requirements  
for the degree of  
Doctor of Philosophy**

**April 2019**

## ACKNOWLEDGEMENT

In the name of Allah, the Beneficent, the Merciful. I start to express my heartfelt gratitude and greatest appreciation to my supervisor Prof. Dr. Mohd Azmier Ahmad who had given valuable guidance and constant support. His invaluable help of constructive comments and suggestions throughout the experimental and thesis works have contributed to the success of this research.

I would also like to express my deepest gratitude to University Malaysia Perlis together with Ministry of Higher Education for funding my PhD study. I am also indebted to Universiti Sains Malaysia under the Iconic grant scheme (Grant No. 1001/CKT/ 870023) for research associated with the Solid Waste Management Cluster, Bridging grant (304. PJKIMIA. 6316100) and Bridging grant (304. PJKIMIA. 60312032) for funding this project. I would like to thank all the technicians and postgraduate students of School of Chemical Engineering for their kindness assistance, professional advice and guidance along completing my thesis.

My special appreciation goes to my dearest husband Mohd Ridzuan bin Mohd Jamir and my daughter Dhia Adelia bt Mohd Ridzuan for their love, support, and encouragement. Not forgotten to both of my beloved parents Khasri bin Md Nen and Sandiah binti Depong, as well as my other family members for their continuous love and support. Last but not least, I would like to thank all the people who have helped me through my research, directly or indirectly; their contribution shall not be forgotten.

*Azduwin binti Khasri*  
*January 2019*

## TABLE OF CONTENTS

	Page
<b>ACKNOWLEDGEMENT</b>	<b>ii</b>
<b>TABLE OF CONTENTS</b>	<b>iii</b>
<b>LIST OF TABLES</b>	<b>vii</b>
<b>LIST OF FIGURES</b>	<b>x</b>
<b>LIST OF SYMBOLS</b>	<b>xv</b>
<b>LIST OF ABBREVIATIONS</b>	<b>xviii</b>
<b>ABSTRAK</b>	<b>xix</b>
<b>ABSTRACT</b>	<b>xx</b>
<b>CHAPTER 1: INTRODUCTION</b>	<b>1</b>
1.1 Background of study	1
1.2 Problem statement	3
1.3 Research objectives	5
1.4 Scope of study	6
1.5 Thesis outline	7
<b>CHAPTER 2: LITERATURE REVIEW</b>	<b>8</b>
2.1 Synthetic dyes and toxicity	8
2.2 Textile effluents and regulation	10
2.3 Dyes removal techniques	12
2.4 Adsorption	14
2.5 Activated carbon	15
2.5.1 Source of AC	16
2.5.2 Wood residues as a precursor	16
2.5.3 Classification of porous materials	18
2.6 Production of AC	21
2.6.1 Carbonization process	21
2.6.2 Activation process	22
2.6.2 (a) Physical activation	22
2.6.2 (b) Chemical activation	23
2.6.2 (c) Physicochemical activation	24
2.7 Microwave heating activation	24
2.8 Factors affecting microwave induced chemical activation	30
2.8.1 Effects of microwave radiation power	30

2.8.2 Effects of microwave radiation time	31
2.8.3 Effects of IR	33
2.9 Optimization of AC preparation conditions and RSM method	34
2.10 Adsorption isotherm	36
2.10.1 Langmuir isotherm	37
2.10.2 Freundlich isotherm	38
2.10.3 Temkin isotherm	39
2.10.4 Dubinin-Radushkevich isotherm	39
2.11 Adsorption kinetics	40
2.11.1 Pseudo-first order kinetic model	41
2.11.2 Pseudo-second order kinetic model	41
2.11.3 Elovich kinetic model	42
2.11.4 Avrami kinetic model	43
2.12 Adsorption mechanism	43
2.12.1 Weber–Morris intraparticle diffusion mechanism	44
2.12.2 Boyd plot diffusion mechanism model	45
2.13 Adsorption thermodynamics	46
2.14 Continuous adsorption	47
2.14.1 Fixed-bed column studies	47
2.14.2 Breakthrough curve modeling	50
2.14.2 (a) Adams-Bohart model	50
2.14.2 (b) Thomas Model	51
2.14.2 (c) Yoon–Nelson model	51
2.15 Regeneration	52
<b>CHAPTER 3: MATERIALS AND METHODS</b>	<b>54</b>
3.1 Experimental overview	54
3.2 Materials	56
3.3 Equipment and instrumentations	58
3.3.1 AC preparation system	58
3.3.2 Characterization system	60
3.3.2 (a) Nitrogen adsorption-desorption isotherms	60
3.3.2 (b) Proximate analysis	61
3.3.2 (c) Ultimate analysis	61
3.3.2 (d) Surface morphology analysis	61
3.3.2 (e) Surface chemistry determination	62

3.3.3 Batch adsorption systems	62
3.3.4 Column adsorption system	63
3.3.5 Analysis system	64
3.4 Experimental procedure	64
3.4.1 Preparation of AC	64
3.4.2 Design of experiment for preparation of ACs	65
3.4.3 Batch adsorption equilibrium studies	67
3.4.3 (a) Effect of contact time and initial concentration	68
3.4.3 (b) Effect of solution temperature	69
3.4.3 (c) Effect of initial solution pH	69
3.4.4 Adsorption isotherm model	70
3.4.5 Batch adsorption kinetics	70
3.4.6 Adsorption mechanism	71
3.4.7 Thermodynamic studies	71
3.4.8 Fixed bed adsorption studies	72
3.4.9 Regeneration of the spent ACs	72
<b>CHAPTER 4: RESULTS AND DISCUSSION</b>	<b>74</b>
4.1 Experimental design	74
4.1.1 Regression model development on PSAC	74
4.1.2 Response surface of PSAC in 3D	80
4.1.3 Regression model development of ISAC	83
4.1.4 Response surface of ISAC in 3D	88
4.1.5 Regression model development of HSAC	90
4.1.6 Response surface of HSAC in 3D	95
4.1.7 Comparison of PSAC, ISAC and HSAC performance	97
4.1.7 (a) Interpretation of regression analysis	97
4.1.7 (b) 3D response surface	99
4.1.7 (c) Process optimization and validation	99
4.2 Characterization of sawdust, char and ACs	102
4.2.1 Surface area and pore characteristics	102
4.2.2 Proximate and elemental analysis	106
4.2.3 Surface morphology	108
4.2.4 Surface chemistry	110
4.3 Batch adsorption studies	113

4.3.1 Equilibrium studies	113
4.3.1 (a) Effect of contact time and initial concentration	114
4.3.1 (b) Effect of solution temperature	118
4.3.1 (c) Effect of initial solution pH	120
4.3.2 Isotherm studies	123
4.3.3 Kinetic studies	136
4.3.4 Adsorption mechanism	149
4.3.4 (a) Weber–Morris intraparticle diffusion	149
4.3.4 (b) Boyd models	154
4.3.4 (c) Pore filling and interaction	158
4.3.5 Thermodynamic studies	163
4.3.6 Summary on the mechanism of ACs	164
4.4 Fixed bed column studies	165
4.4.1 Effect of volumetric flow rate	165
4.4.2 Effect of initial concentration	168
4.4.3 Effect of bed height	171
4.4.4 Comparison on all ACs performance for MB and RBV adsorption	174
4.4.5 Breakthrough modelling	176
4.5 Spent ACs regeneration	178
<b>CHAPTER 5: CONCLUSION AND RECOMMENDATIONS</b>	<b>181</b>
5.1 Conclusions	181
5.2 Recommendations	183
<b>REFERENCES</b>	<b>184</b>
<b>APPENDICES</b>	
Appendix A: Calibration curve for MB and RBV dyes	
Appendix B: Preliminary studies	
Appendix C: Proximate and elemental analysis	
Appendix D: Plots of adsorption uptakes versus time	
Appendix E: Plots of percentage removal versus time	
Appendix F: Amount of dyes adsorbed and removal	
Appendix G: Parameters of kinetics	
Appendix H: Parameters of intraparticle diffusion model	
Appendix I : Boyd plots	
Appendix J : Thermodynamic plot	
<b>LIST OF PUBLICATIONS AND AWARDS</b>	

## LIST OF TABLES

	<b>Page</b>
Table 2.1 Acceptable conditions for discharge of industrial effluent for mixed effluent of standards A and B (Department of Environment Malaysia, 2010)	11
Table 2.2 Advantages and disadvantages of dye removal methods	13
Table 2.3 Comparison of physisorption and chemisorption	15
Table 2.4 Steps and range of temperature in the carbonization process (Chowdhury et al., 2013)	22
Table 2.5 Advantages and disadvantages of microwave and conventional heating	27
Table 2.6 Previous studies using microwave heating activation for basic dye adsorption	29
Table 2.7 Previous studies using microwave heating activation for reactive dye adsorption	29
Table 2.8 Effects of IR (microwave power = 800 W; activation time = 9 minutes) (Li et al., 2016)	34
Table 2.9 Optimization parameter of different adsorbent	36
Table 2.10 Regeneration efficiency of various adsorbents in previous work	53
Table 3.1 List of reagents and chemicals	56
Table 3.2 Properties of MB	57
Table 3.3 Properties of RBV	57
Table 3.4 Complete design matrix for AC preparation	66
Table 4.1 Experimental design matrix for preparation of PSAC	75
Table 4.2 ANOVA and lack of fit test for response surface quadratic model for MB removal of PSAC	78
Table 4.3 ANOVA and lack of fit test for response surface quadratic model for RBV removal of PSAC	79
Table 4.4 ANOVA and lack of fit test for response surface quadratic model for PSAC yield	80

Table 4.5	Experimental design matrix for preparation of ISAC	83
Table 4.6	ANOVA and lack of fit test for response surface quadratic model for MB removal of ISAC	86
Table 4.7	ANOVA and lack of fit test for response surface quadratic model for RBV removal of ISAC	86
Table 4.8	ANOVA and lack of fit test for response surface quadratic model for ISAC yield	87
Table 4.9	Experimental design matrix for preparation of HSAC	90
Table 4.10	ANOVA and lack of fit test for response surface quadratic model for MB removal of HSAC	93
Table 4.11	ANOVA and lack of fit test for response surface quadratic model for RBV removal of HSAC	93
Table 4.12	ANOVA and lack of fit test for response surface quadratic model for HSAC yield	94
Table 4.13	Significant factor for PSAC, ISAC and HSAC from ANOVA	97
Table 4.14	Model validation for ACs prepared for MB removal and yield	101
Table 4.15	Model validation for AC prepared for RBV removal and yield	101
Table 4.16	Surface area and pore characteristics of the samples	104
Table 4.17	Isotherm parameters for adsorption of MB dyes by optimized PSAC, ISAC and HSAC at 30, 45 and 60 °C	131
Table 4.18	Isotherm parameters for adsorption of RBV dyes by optimized PSAC, ISAC and HSAC at 30, 45 and 60 °C	132
Table 4.19	Kinetic parameters for MB-PSAC, MB-ISAC and MB-HSAC systems at 30 °C	145
Table 4.20	Kinetic parameters for RBV-PSAC, RBV-ISAC and RBV-HSAC systems at 30 °C	147
Table 4.21	Intraparticle diffusion model constant and $R^2$ values for adsorption of MB-PSAC, MB-ISAC and MB-HSAC at 30 °C	153
Table 4.22	Intraparticle diffusion model constant and $R^2$ values for adsorption of RBV onto PSAC, ISAC and HSAC at 30 °C	154



Table 4.23	Boyd plot diffusion coefficients of MB adsorption onto PSAC, ISAC and HSAC at 30 °C	157
Table 4.24	Boyd plot diffusion coefficients of RBV adsorption onto on PSAC, ISAC and HSAC at 30 °C	157
Table 4.25	Thermodynamic parameters for MB and RBV dyes adsorption onto optimized ACs	163
Table 4.26	Summary of the type of adsorption for PSAC, ISAC and HSAC for MB and RBV adsorption	164
Table 4.27	Column data parameters for adsorption of MB onto PSAC, ISAC and HSAC	174
Table 4.28	Column data parameters for adsorption of RBV onto PSAC, ISAC and HSAC	175
Table 4.29	Parameters predicted from the Adams-Bohart model for MB and RBV adsorption by PSAC, ISAC and HSAC	177
Table 4.30	Parameters predicted from the Thomas model for MB and RBV adsorption by PSAC, ISAC and HSAC	177
Table 4.31	Parameters predicted from the Yoon-Nelson model for MB and RBV adsorption by PSAC, ISAC and HSAC	178
Table 4.32	Regeneration efficiency of MB and RBV onto spent PSAC, ISAC and HSAC	179

## LIST OF FIGURES

		<b>Page</b>
Figure 2.1	Porous structure of AC (Suresh Kumar et al., 2017)	19
Figure 2.2	Type of adsorption isotherm (Zhang et al., 2016).	20
Figure 2.3	Classification of hysteresis loops and their related pore shapes (Zhang et al., 2016)	21
Figure 2.4	Schematic of temperature profile and direction of heat transfer (a) conventional heating (b) microwave heating (red-high temperature, blue-low temperature) (Lin and Chen, 2015)	25
Figure 2.5	Comparison between conventional & microwave chemical activation process towards surface characteristics of various precursors (Liu et al., 2010; Xin-hui et al., 2011; Alslaibi et al., 2014; Sharif et al., 2018)	28
Figure 2.6	Effects of microwave power (H <sub>3</sub> PO <sub>4</sub> concentration = 40%; activation time = 8 min) (Duan et al., 2016)	31
Figure 2.7	Effects of activation time (microwave power = 640 W; H <sub>3</sub> PO <sub>4</sub> concentration = 40% (c) (Duan et al., 2016)	33
Figure 2.8	The schematic diagram of the adsorption process and mechanism (Feng et al., 2012)	45
Figure 2.9	Typical breakthrough curve (Kopsidas, 2018)	48
Figure 3.1	Schematic flow diagram of experimental activities	55
Figure 3.2	Waste sawdust from (a) PS (b) IS and (c) HS	56
Figure 3.3	Schematic diagram of the carbonization unit	58
Figure 3.4	Schematic diagram of the microwave activation unit	59
Figure 3.5	Schematic diagram of adsorption column system	63
Figure 4.1	Predicted versus actual experimental values for (a) MB removal, (b) RBV removal and (c) PSAC yield	77
Figure 4.2	3D response plot for (a) MB removal (effect of radiation power and IR, radiation time = 4 min), (b) RBV removal (effect of radiation power and IR, radiation time = 4	81

	min) and (c) PSAC yield (effect of radiation power and radiation time, IR = 0.5)	
Figure 4.3	Predicted versus actual experimental values for (a) MB removal, (b) RBV removal and (c) ISAC yield.	85
Figure 4.4	3D response plot for (a) MB removal (effect of radiation power and IR, radiation time = 4 min), (b) RBV removal (effect of radiation power and IR, radiation time = 4 min) and (c) ISAC yield (effect of radiation power and radiation time, IR = 0.5)	89
Figure 4.5	Predicted versus actual experimental values for (a) MB removal, (b) RBV removal and (c) HSAC yield.	92
Figure 4.6	3D response plot for (a) MB removal (effect of radiation power and IR, radiation time = 4 min), (b) RBV removal (effect of radiation power and IR, radiation time = 4 min) and (c) HSAC yield (effect of radiation power and radiation time, IR = 0.5)	96
Figure 4.7	Profile for surface area of (a) PSAC (b) ISAC and (c) HSAC	103
Figure 4.8	Pore size distributions of PSAC, ISAC and HSAC	105
Figure 4.9	Proximate analysis of the samples (a) before and (b) after activation	107
Figure 4.10	Elemental analysis of the samples (a) before and (b) after activation	108
Figure 4.11	SEM images of (a) PS, (b) PS char and (c) PSAC (magnification of 1kx)	109
Figure 4.12	SEM images of (a) IS, (b) IS char and (c) ISAC (magnification of 1kx)	109
Figure 4.13	SEM images of (a) HS, (b) HS char and (c) HSAC (magnification of 1kx)	109
Figure 4.14	FTIR spectrum for PS and PSAC	110
Figure 4.15	FTIR spectrum for MR and ISAC	111
Figure 4.16	FTIR spectrum for HS and HSAC	113
Figure 4.17	MB adsorption uptake versus adsorption time at various initial concentrations by (a) MB-PSAC, (b) MB-ISAC and (c) MB-HSAC at 30 °C	115

Figure 4.18	RBV adsorption uptake versus adsorption time at various initial concentrations by (a) RBV-PSAC, (b) RBV-ISAC and (c) RBV-HSAC at 30 °C	116
Figure 4.19	Effect of solution temperature on MB adsorption capacity of MB-PSAC, MB-ISAC and MB-HSAC systems (condition: initial concentration 100 mg/L)	119
Figure 4.20	Effect of solution temperature on RBV adsorption capacity of RBV-PSAC, RBV-ISAC and RBV-HSAC systems (condition: initial concentration 100 mg/L)	119
Figure 4.21	Effect of initial pH on MB adsorption capacity by optimized PSAC, ISAC and HSAC	120
Figure 4.22	The AC–MB dye interaction under different pH conditions: (a) basic and (b) acidic	121
Figure 4.23	Effect of initial pH on RBV adsorption capacity by optimized PSAC, ISAC and HSAC	122
Figure 4.24	The AC–RBV dye interaction under different pH conditions: (a) basic and (b) acidic	123
Figure 4.25	Plots of (a) Langmuir, (b) Freundlich, (c) Temkin and (d) Dubinin-Radushkevich for MB adsorption onto optimized PSAC at 30, 45 and 60 °C	124
Figure 4.26	Plots of (a) Langmuir, (b) Freundlich, (c) Temkin and (d) Dubinin-Radushkevich for MB adsorption onto optimized ISAC at 30, 45 and 60 °C	125
Figure 4.27	Plots of (a) Langmuir, (b) Freundlich, (c) Temkin and (d) Dubinin-Radushkevich for MB adsorption onto optimized HSAC at 30, 45 and 60 °C	126
Figure 4.28	Plots of (a) Langmuir, (b) Freundlich, (c) Temkin and (d) Dubinin-Radushkevich for RBV adsorption onto optimized PSAC at 30, 45 and 60 °C	127
Figure 4.29	Plots of (a) Langmuir, (b) Freundlich, (c) Temkin and (d) Dubinin-Radushkevich for RBV adsorption onto optimized ISAC at 30, 45 and 60 °C	128
Figure 4.30	Plots of (a) Langmuir, (b) Freundlich, (c) Temkin and (d) Dubinin-Radushkevich for RBV adsorption onto optimized HSAC at 30, 45 and 60 °C	129
Figure 4.31	Plots of separation factor, $RL$ versus MB initial concentration for optimized PSAC, ISAC and HSAC at (a) 30 °C, (b) 45 °C and (c) 60 °C	133

Figure 4.32	Plots of separation factor, RL versus RBV initial concentration for optimized PSAC, ISAC and HSAC at (a) 30 °C, (b) 45 °C and (c) 60 °C	134
Figure 4.33	Linearized plots of pseudo-first order kinetic model for (a) MB-PSAC, (b) MB-ISAC and (c) MB-HSAC systems at 30 °C	137
Figure 4.34	Linearized plots of pseudo-second order kinetic model for (a) MB-PSAC, (b) MB-ISAC and (c) MB-HSAC systems at 30 °C	138
Figure 4.35	Linearized plots of Elovich kinetic model for (a) MB-PSAC, (b) MB-ISAC and (c) MB-HSAC systems at 30 °C	139
Figure 4.36	Linearized plots of Avrami kinetic model for (a) MB-PSAC, (b) MB-ISAC and (c) MB-HSAC systems at 30 °C	140
Figure 4.37	Linearized plots of pseudo-first order kinetic model for (a) RBV-PSAC, (b) RBV-ISAC and (c) RBV-HSAC systems at 30 °C	141
Figure 4.38	Linearized plots of pseudo-second order kinetic model for (a) RBV-PSAC, (b) RBV-ISAC and (c) RBV-HSAC systems at 30 °C	142
Figure 4.39	Linearized plots of Elovich kinetic model for (a) RBV-PSAC, (b) RBV-ISAC and (c) RBV-HSAC systems at 30 °C	143
Figure 4.40	Linearized plots of Avrami kinetic model for (a) RBV-PSAC, (b) RBV-ISAC and (c) RBV-HSAC systems at 30 °C	144
Figure 4.41	Plots of intraparticle diffusion model for MB adsorption onto (a) PSAC, (b) ISAC and (c) HSAC	150
Figure 4.42	Plots of intraparticle diffusion model for RBV adsorption onto (a) PSAC, (b) ISAC and (c) HSAC	151
Figure 4.43	Boyd's plots for MB adsorption onto (a) PSAC, (b) ISAC and (c) HSAC at 30 °C	155
Figure 4.44	Boyd's plots for RBV adsorption onto (a) PSAC, (b) ISAC and (c) HSAC at 30 °C	156
Figure 4.45	Chemical structure and molecular dimension of (a) MB and (b) RBV dyes.	159

Figure 4.46	Possible interactions contributing to the mechanism of (a) MB and (b) RBV adsorption onto PSAC, ISAC and HSAC	161
Figure 4.47	Illustration of possible PSAC, ISAC and RSAC components based on elemental analysis (N and S component is negligible)	162
Figure 4.48	Breakthrough curve of MB dyes adsorption onto (a) PSAC, (b) ISAC and (c) HSAC at different flow rate (initial concentration = 100 mg/L and bed height = 2 cm)	166
Figure 4.49	Breakthrough curve of RBV dyes adsorption onto (a) PSAC, (b) ISAC and (c) HSAC at different flow rate (inlet concentration = 100 mg/L and bed height = 2 cm)	167
Figure 4.50	Breakthrough curve of MB dyes adsorption onto (a) PSAC, (b) ISAC and (c) HSAC at different initial concentration (flow rate = 10 mL/min and bed height = 2 cm)	169
Figure 4.51	Breakthrough curve of RBV dyes adsorption onto (a) PSAC, (b) ISAC and (c) HSAC at different flow rate (inlet concentration = 100 mg/L and bed height = 2 cm)	170
Figure 4.52	Breakthrough curve of MB dyes adsorption onto (a) PSAC, (b) ISAC and (c) HSAC at different bed height (initial concentration = 100 mg/L and flow rate = 10 mL/min)	172
Figure 4.53	Breakthrough curve of RBV dyes adsorption onto (a) PSAC, (b) ISAC and (c) HSAC at different flow rate (inlet concentration = 100 mg/L and bed height = 2 cm)	173
Figure 4.54	Regeneration performance of (a) MB-PSAC, (b) MB-ISAC and (c) MB-HSAC	179
Figure 4.55	Regeneration performance of (a) RBV-PSAC, (b) RBV-ISAC and (c) RBV-HSAC	180

## LIST OF SYMBOLS

	<b>Symbol</b>	<b>Unit</b>
A	Arrhenius pre-exponential factor	-
$A_T$	Temkin isotherm constant	L/g
$b_i$	Linear coefficient	-
$b_0$	Constant coefficient	-
$b_{ii}$	Quadratic coefficient	-
$b_{ij}$	Interaction coefficient	-
B	Boyd plot slope	-
$B_{DR}$	Dubinin–Radushkevich model constant	$\text{mol}^2 / \text{kJ}^2$
$B_T$	Temkin constant related to the heat of adsorption	J/mol
$B_t$	Boyd plot constant	-
C	Intercept related to the boundary layer effect	mg/g
$C_e$	Adsorbate concentration at equilibrium	mg/L
$C_0$	Adsorbate concentration at initial	mg/L
$C_t$	Adsorbate concentration at time “t”	mg/L
$C_{ad}$	Adsorbed solute concentration	mg/L
$D_i$	Effective diffusion coefficient	$\text{m}^2/\text{h}$
$e_i$	Error	-
$E_a$	Activation energy	kJ/mol
$E_{DR}$	Mean energy of sorption	kJ/mol
H	The bed depth of column	cm
$k_A$	Adams-Bohart kinetic constant	L/min.mg
$k_{TH}$	Thomas rate constant	L/min mg
$k_Y$	Yoon Nelson rate constant	1/min
$k_{AV}$	Avrami constant	1/h
$k_{ti}$	Intraparticle diffusion rate constant	$\text{mg/g h}^{1/2}$
$k_1$	Pseudo-first order model rate constant	1/h
$k_2$	Pseudo-second order rate constant	g/mg h
Kc	The equilibrium constant	-
$K_L$	Langmuir model constant	L/mg

$K_f$	Freundlich constant related to adsorption capacity	$(\text{m/g})(\text{L/mg})^{1/n}$
$m_s$	Dry weight of the adsorbent after exhausted	g
$m_{\text{tot}}$	Quantity of adsorbates deposited in the column	g
$M$	Mass of activated carbon	g
$n$	Number of variables	-
$n_c$	Number of centre runs	-
$n_F$	Freundlich constant related to sorption intensity of the sorbent	-
$n_{AV}$	Avrami model exponent of time	-
$N$	Number of data points	-
$N_0$	Adams-Bohart saturation concentration	mg/L
$q_e$	Amount of adsorbate adsorbed at equilibrium	mg/g
$q_{TH}$	Thomas adsorption capacity of the bed	mg/g
$q_t$	Adsorption capacity of adsorbent at time “t”	mg/g
$q_{\text{bed}}$	Bed capacity	mg/g
$q_{\text{tot}}$	Total adsorbed quantity of adsorbate	mg
$q_{e,\text{exp}}$	Experimental amount of adsorbate adsorbed at equilibrium	mg/g
$q_{e,\text{cal}}$	Calculated amount of adsorbate adsorbed at equilibrium	mg/g
$Q$	Volumetric flow rate	mL/min
$Q_m$	Maximum Langmuir monolayer capacity	mg/g
$Q_{DR}$	Theoretical monolayer saturation capacity	mg/g
$r$	Radius of the adsorbent particle	m
$R$	Perfect gas constant	J/mol.K
$R_L$	Langmuir adsorption isotherm characteristic	-
$R^2$	Correlation coefficient	-
$S_{BET}$	BET surface area	$\text{m}^2/\text{g}$
$t_{\text{tot}}$	Total flow time until exhaustion	min
$T$	Absolute temperature	K
$U_o$	Linear velocity	cm/min
$V$	Volume of the solution	L
$w_{\text{char}}$	Dry weight of char	g
$w_{\text{KOH}}$	Dry weight of KOH pellets	g
$W$	Mass of adsorbent	g
$x_1$	Radiation power	Watt



$x_2$	Radiation time	min
$x_3$	Impregnation ratio	-
$Y_1$	Percentage of adsorbate removal	%
$Y_2$	Yield percentage	%

#### Greek letters

$\pm\alpha$	Distance of axial point from centre	-
$\alpha_E$	Elovich initial adsorption rate	mg/g min
$\beta_E$	Elovich desorption constant	g/mg
$\Delta G^\circ$	Change in free energy	kJ/mol
$\Delta H^\circ$	Change in enthalpy	kJ/mol
$\Delta S^\circ$	Change in entropy	kJ/mol
$\Delta q$	The normalised standard deviation	-
$\varepsilon$	Polanyi potential	kJ/mol
$\lambda$	Wavelength	nm
$\pi$	Ratio of a circle's circumference to its diameter	-
$\tau$	Time required for 50% adsorbate breakthrough	min
$\chi^2$	Chi-square	-

## LIST OF ABBREVIATIONS

AC	Activated carbon
ANOVA	Analysis of variance
AP	Adequate Precision
BET	Brunauer-Emmett-Teller
CCD	Central composite design
DoE	Design of experiment
FC	Fixed carbon
FRIM	Forest Research Institute Malaysia
FTIR	Fourier transform infrared
HS	<i>Hevea brasiliensis</i> sawdust
HSAC	<i>Hevea brasiliensis</i> sawdust-based activated carbon
IR	Impregnation ratio
IS	<i>Intsia bijuga</i> sawdust
ISAC	<i>Intsia bijuga</i> sawdust-based activated carbon
IUPAC	International Union of Pure and Applied Chemistry
MB	Methylene blue
MTZ	Mass transfer zone
PS	<i>Pentace triptera</i> sawdust
PSAC	<i>Pentace triptera</i> sawdust-based activated carbon
RBV	Reactive Brilliant Violet 5R
rpm	Rotation per minute
RSM	Response surface methodology
SD	Standard deviation
SEM	Scanning electron microscopy
spp.	Species
TGA	Thermogravimetric analyzer
VM	Volatile matter

**KARBON TERAKTIF DARIPADA HABUK KAYU *PENTACE TRIPTERA*,  
*INTSIA BIJUGA* DAN *HEVEA BRASILIENSIS* TERHASIL MELALUI  
PENGAKTIFAN GELOMBANG MIKRO TERINDUKSI KALIUM  
HIDROKSIDA UNTUK PENYERAPAN PEWARNA**

**ABSTRAK**

Pewarna sintetik digunakan secara meluas dalam pelbagai industri yang mengakibatkan pencemaran air. Oleh itu, kajian ini bertujuan untuk menghasilkan karbon teraktif (AC) daripada *Pentace triptera* (PS), *Intsia bijuga* (IS) dan *Hevea brasiliensis* (HS) untuk penjerapan pewarna metilena biru (MB) dan remazol ungu berkilau 5R (RBV) melalui pengaktifan gelombang mikro-terinduksi kalium hidroksida (KOH) bersama dengan gasifikasi karbon dioksida (CO<sub>2</sub>). Keadaan penyediaan optimum untuk semua AC ditentukan menggunakan kaedah permukaan respon (RSM). ISAC telah menunjukkan luas permukaan Brunauer-Emmet-Teller (BET) dan jumlah jisim liang yang tinggi iaitu 952.23 m<sup>2</sup>/g dan 0.584 cm<sup>3</sup>/g, masing-masing berbanding PSAC dan HSAC. Semua penjerap berpadanan dengan model isoterma Langmuir dengan ISAC telah menunjukkan kapasiti penjerapan monolayer maksimum (Q<sub>m</sub>) tertinggi sebanyak 434.78 dan 212.77 mg/g, masing-masing untuk pewarna MB dan RBV pada 30°C. Kajian kinetik menunjukkan bahawa semua sistem mengikuti model pseudo-tertib kedua dengan resapan filem adalah langkah pengehad yang mengawal penjerapan. Kajian termodinamik mengesahkan bahawa semua sistem bersifat endotermik. Untuk kajian turus, korelasi data terobosan yang lebih baik ditunjukkan oleh model Thomas dan Yoon-Nelson. Semua AC mempunyai prestasi kebolegunaan yang baik untuk penjerapan MB dan RBV terutamanya sehingga tiga kitaran menggunakan etanol sebagai pelarut.

**ACTIVATED CARBON DERIVED FROM *PENTACE TRIPTERA*, *INTSIA*  
*BIJUGA* AND *HEVEA BRASILIENSIS* SAWDUST VIA MICROWAVE-  
INDUCED POTASSIUM HYDROXIDE ACTIVATION FOR DYES  
ADSORPTION**

**ABSTRACT**

Synthetic dyes are widely applied in various industries which has resulted in the water pollution. Therefore, this study aims to synthesis activated carbon (AC) from *Pentace triptera* (PS), *Intsia bijuga* (IS) and *Hevea brasiliensis* (HS) for methylene blue (MB) and remazol brilliant violet 5R (RBV) dye adsorption via microwave-induced potassium hydroxide (KOH) activation adopted together with carbon dioxide (CO<sub>2</sub>) gasification. Optimum preparation conditions for all ACs prepared were determined using response surface methodology (RSM). ISAC showed high Brunauer-Emmet-Teller (BET) surface area and total pore volume of 952.23 m<sup>2</sup>/g and 0.584 cm<sup>3</sup>/g, respectively compared to PSAC and HSAC. All adsorbents best fitted to the Langmuir isotherm model with ISAC showed higher maximum monolayer adsorption capacity (Q<sub>m</sub>) of 434.78 and 212.77 mg/g, respectively for MB and RBV dye at 30°C. Kinetic studies showed that all system followed a pseudo-second order model with film diffusion was the rate-limiting step controlling adsorption. Thermodynamic studies confirmed that all systems were endothermic in nature. For the column studies, the better correlation of breakthrough data shown by Thomas and Yoon-Nelson model. The ACs had good reusability performance for MB and RBV adsorption especially up to three cycle using ethanol as solvent.

# CHAPTER 1

## INTRODUCTION

This chapter highlights the background of the study, problem statement, research objectives as well as scope of study.

### 1.1 Background of study

Dyes are common pollutants that can be found in aqueous waste streams from industrial sections including paint, textile, plastic, cosmetic and paper industries. Greater than 700,000 metric tons of dyes are produced annually, with 2-3% is reported loss to industrial wastewaters during manufacturing and dyeing (Sangon *et al.*, 2018). Many of these dyes can cause allergies, skin irritation or even cancer and human mutations (Wang *et al.*, 2018). They are also considered dangerous to the environment and result in the deterioration of water quality, thus affecting aquatic life (Heidarinejad *et al.*, 2018). It is therefore essential to remove these dyes from the waste stream prior to release into watercourses.

Various methods such as adsorption, coagulation, advanced oxidation and membrane separation are used in the removal of dyes from wastewater. Adsorption via activated carbon (AC) as adsorbent is one of the most effective wastewater treatment processes used by the textile industry to reduce pollutants present in the effluent (Yagub *et al.*, 2014). AC is a term used to express carbon-rich materials which contain well-built internal pore structure. The high surface area ( $> 400 \text{ m}^2/\text{g}$ ), well-organized pores and a wide range of chemical functional groups present on the surface of AC make it a versatile and popular adsorbent in wastewater treatment industries (Danish and Ahmad, 2018).

Recently, heating systems employing microwave irradiation have been widely used for the preparation of AC. The microwave energy is transferred to the interior part of the samples by dipole rotation and ionic conduction, rather than by conduction and convection (Makhado *et al.*, 2018). Consequently, microwave heating results in a significantly reduced treatment time. The removal of dyes from wastewater using AC prepared by microwave-assisted activation from various source such as date stones (Abbas and Ahmed, 2016), coconut shells (Mohammed *et al.*, 2015), pomegranate peel (Ahmad *et al.*, 2014), oil palm shells (Hesas *et al.*, 2013a), peanut shells (Georgin *et al.*, 2016), coffee shells (Li *et al.*, 2016a), palm kernel shells (Kundu *et al.*, 2015a), *Jatropha* (Khalil *et al.*, 2013) and rice husks (Muniandy *et al.*, 2014) have been studied by other researchers. Out of these presursors, woody materials are significant sources for AC preparation, because they contain appropriate carbon fractions (50–90%) and low ash content (< 5 %) (Kazemi *et al.*, 2016).

Malaysia produces large amount of forest and wood processing mass where logging residues were produced during various phases of logging. The secondary processing residues are produced during the process of planning mills, moulding plants, and furniture factories in the form of sawdust, plane shavings, small pieces of lumber trimming, edging, bark and fragments (Osman *et al.*, 2014). With the growing of wood activities has also increased the wood waste amount resulted from this process. *Pentace triptera* (PS), *Intsia bijuga* (IS) and *Hevea brasiliensis* (HS) are among commercially important hardwoods used in Malaysian wooden furniture manufacturing industry which has resulted in the increasing of the waste sawdust from these wood species. These three woods PS, IS and HS possess different density of 530-755 kg/m<sup>3</sup>, 515-1,040 kg/m<sup>3</sup> and 560 - 640 kg/m<sup>3</sup>, respectively. It was hypothesized that different density of wood will results in different characteristic and adsorption

capability for batch and column mode of studies. Therefore, the potential of these three waste sawdust as a precursor in producing novel AC has been explored in this study.

## 1.2 Problem statement

Various cationic and anionic synthetic dyes such as methylene blue (MB) and Remazol Brilliant Violet 5R (RBV) are released in water bodies through the effluents of these industries. The discharge of MB basic dye into the water stream has a number of harmful effects such as allergic dermatitis, skin irritation, mutations, and even cancer (Rangabhashiyam and Balasubramanian, 2018). The reactive RBV dye is an anthracene derivative and represents an important class of toxic and recalcitrant organic pollutants (Bello and Ahmad, 2011a). Due to stable conjugation structures by the presence of an -N=N- (azo) bond in the chemical structure, RBV dye is difficult to eliminate by biodegradation process (Li *et al.*, 2017). Therefore, the strategy to eliminate the colour and to reduce its effect on the industrial effluents before they are mixed up with natural water bodies is of significant importance.

Adsorption process using AC has been considered superior method for dye treatment due its high efficiency and operational simplicity. However, this application is limited by the cost of production and vague methods (Danish and Ahmad, 2018). The heating techniques strongly affect the physical and chemical characteristics of AC. Through conventional heating, heat is transferred to the samples by conduction and convection mechanisms which leads to an inhomogeneous heating samples of dissimilar shapes and sizes. Furthermore, this thermal heating takes a longer time to achieve the preferred phase of activation. Consequently, volatile components may remain inside the particles, giving rise to carbon deposition problems. The deposited carbon leading to distortion and inhomogeneous structure, low values of total pore

volume and BET surface area (Ao *et al.*, 2018). Therefore, microwave heating technique was used in the present work which can ensure a uniform heating, short activation time and good porosity.

The existing AC derived from coal are limited and non-renewable. Therefore, the paradigm shifted towards renewable resources. Heap of sawdust is created on regular basis at sawmills which consequently continues to create solid waste management problem. The easiest way commonly adopted by most sawmill operators to get rid of the sawdust is open burning which has been known to be associated with emission of air pollutants. Approximately 75% of wood residues generated by sawmills are utilized while the remaining 25% are still disposed of or by incineration (Yoshida and Suzuki, 2010). PS, IS and HS are among the three type of commercially important hardwoods used in the wooden furniture manufacturing industry with high consumption of logs record of 17877 m<sup>3</sup>, 73510 m<sup>3</sup> and 89809 m<sup>3</sup>, respectively (Forestry Department Peninsular Malaysia, 2016). The volume of sawdust from sawmills continues to increase due to a rise in lumber production to meet growing demand for this type of wood products. Thus, in this study, the potential of unutilized waste sawdust especially from PS, IS and HS was explored in producing ACs.

At present, AC are mostly synthesized using “one-parameter-at-a-time” approach, whereby the parameter of interest is varied whilst the other parameters are fixed. Nevertheless, the conventional approach is time-consuming, making it unfavourable from the economic perspective. The approach also fails to describe the interaction of these parameters with the chosen response (Rashidi and Yusup, 2017). Therefore, in the effort to minimize the total number of experimental runs, processing time, and physical effort, a useful tool called as RSM were employed for developing, improving and optimizing the preparation condition of AC.



Fixed bed absorption offers many advantages such as adsorption effectiveness, easy operation, possibility to achieved high capacity, and removal efficiency and can be simply scaled up for industrial (Franco *et al.*, 2017). However, there are limited studies in both batch and column mode for dyes adsorption. Therefore, the present work focuses on the potential of PS, IS and HS based AC which produced via microwave-induced KOH activation in the removal of MB and RBV dye from aqueous solution using both batch and fixed bed column processes.

### **1.3 Research objectives**

The objectives of the research include:

- i. To analyze and compare the optimum operating parameters in the preparation of ACs from waste sawdust (PS, IS and HS) via microwave-induced KOH activation and CO<sub>2</sub> gasification for the removal of MB and RBV dyes from aqueous solutions using response surface methodology (RSM).
- ii. To evaluate and compare the characteristic of the optimized ACs in terms of surface area, pore characteristic, surface morphology, surface chemistry, proximate content and elemental analysis.
- iii. To evaluate and compare the effect of contact time, initial concentration, solution temperature, initial solution pH, adsorption isotherm, kinetic, mechanism and thermodynamic for the adsorption of MB and RBV dyes onto optimized ACs in batch adsorption mode.
- iv. To evaluate and compare the effect of volumetric flow rate, initial concentration, and bed height as well as breakthrough modelling for the adsorption of MB and RBV dyes onto optimized ACs in continuous adsorption mode.

#### 1.4 Scope of study

Waste sawdust from PS, IS and HS were first carbonized in tubular furnace in order to produce char. The samples were then converted into ACs via microwave induced KOH and CO<sub>2</sub> gasification. The variable process parameters involved radiation power (264 - 616 W), radiation time (4 - 8 min) and IR (0.5 - 2) were optimized to maximize the yield of AC and its removal efficiency on MB and RBV dyes using RSM adopting central composite design (CCD). The optimized ACs were then characterize in terms of surface area, pore characteristic, surface morphology, surface chemistry, proximate content and elemental analysis. For batch mode, the effects of contact time (0 - 24 hours), initial concentration (25 - 300 mg/L), solution temperature (30 - 60 °C) and initial solution pH (2 - 12) on dyes removal performance were evaluated. Further studies on isotherms (Langmuir, Freundlich, Temkin and Dubinin–Radushkevich), kinetics (Pseudo-first order, Pseudo-second order, Elovich and Avrami), mechanism (Weber-Morris intraparticle diffusion model and Boyd's plot) and thermodynamic were also included. For continuous mode, the effects of different fixed-bed conditions, including volumetric flow rate (5 - 15 mL/min), initial concentration (50 - 150 mg/L) and bed height (2 - 6 cm) were studied. The breakthrough curves were plotted and were analyzed using three models namely Adams–Bohart, Thomas and Yoon–Nelson models. The feasibility of regenerating the exhausted ACs saturated with MB and RBV dyes were determined using ethanol desorption method.

## **1.5 Thesis outline**

This thesis is structured into five chapters and summarized as follows:

Chapter 1 provides the background of the study, problem statement, research objectives and scope of study.

Chapter 2 gives a reviews of literature pertaining to synthetic dyes and toxicity, textile effluents and regulation and dye removal techniques. The fundamental of AC adsorption, carbonization, activation process, microwave heating and optimization using RSM are outlined. Adsorption isotherm, kinetics, mechanism and thermodynamics are also been highlighted in this chapter. The last section explains the breakthrough modeling for fixed-bed column studies.

Chapter 3 describes in detail all the materials and equipment used in the present study. The experimental set up and experimental procedure which includes the preparation of AC, design of experiments, batch and continuous process are also included.

Chapter 4 is divided into five sections which are (i) experimental design and optimization results, (ii) characterization results, (iii) batch adsorption studies, (iv) fixed bed column studies and (v) regeneration.

Chapter 5 concludes the findings from this study. Several recommendations are presented for related upcoming research works in the study field.

## **CHAPTER 2**

### **LITERATURE REVIEW**

This chapter presents a reviews of literature pertaining to synthetic dyes and toxicity, textile effluents and regulation and dye removal techniques. The fundamental of AC adsorption, carbonization, activation process, microwave heating and optimization using RSM are outlined. Adsorption isotherm, kinetics, mechanism and thermodynamics are also been highlighted in this chapter. The last section explains the breakthrough modeling for fixed-bed column studies.

#### **2.1 Synthetic dyes and toxicity**

Synthetic dyes are a chemical compound that is widely used in many important industries such as leather, paper and textile industry due to the need for colour properties of the material. Among other dye-utilizing industries, the textile industry is said to utilize the highest amount of dyestuff at approximately 10 000 tonnes per year worldwide (Jain and Gogate, 2018). The textile industry is the industry that produces a lot of wastewater that contains a number of pollutants including acidic waste, toxic compounds, and various dyes.

Two class of synthetic dyes namely cationic (all basic dyes) and anionic (direct, acid, and reactive) dyes are greatly applied in the fabric productions (Saleh and Gupta, 2014). Cationic dyes carry a positive charge in their molecule, furthermore it is water soluble and yield coloured cations in solution. Basic dyes considered as cationic dyes. Basic dye are toxic and can cause allergic dermatitis, skin irritation, mutations and even cancer (Mohammad *et al.*, 2018). Also, cationic dyes can cause increased in heart rate, shock, vomiting, cyanosis, jaundice, quadriplegia, heinz body

formation and tissue necrosis in humans (Hazzaa and Hussein, 2015). Basic methylene blue (MB) dye with a big heterocyclic aromatic group is a good choice for testing the performance of adsorbents whose mesoporosity suggests their application for adsorption of liquid pollutants. Furthermore, cationic dyes like MB is considered more toxic than anionic ones (Sakin Omer *et al.*, 2018).

Anionic dyes have negative ions due to the excess presence of the OH<sup>-</sup> ions in aqueous solution. Anionic dyes are water soluble and they include acid dyes, direct dyes and reactive dyes. Reactive dyes are common dyes used for dyeing cellulosic fibres due to their favourable characteristics of bright colour, water-fastness, simple application techniques and low energy consumption. They are usually characterized by nitrogen to nitrogen double bonds (N=N azo bonds) where the colour of azo dyes is due to this azo bond and the associated chromophores (Ahmad and Alrozi, 2010). Reactive dyes pose the greatest problem in textiles wastewater since they are not easily biodegradable and thus colour may still remain in the effluent. Reactive remazol brilliant violet (RBV) dye is an anthracene derivative with stable conjugation structures, and thus make it difficult to be eliminated by biodegradation process (Li *et al.*, 2017).

Most of these dyes are carcinogenic, mutagenic, and teratogenic toxic to humans, fish species, and even microorganisms (Aljeboree *et al.*, 2014). Among their environmental impacts, the main issue is related to the reduction of light into the aquatic environment, which in turn leads to a decrease in photosynthetic activity (Wong *et al.*, 2017). In Malaysia, each textile industry factory treats its own wastewater and the treated effluents are normally discharged to a drain but not to a centralized treatment system. Thus, they are compulsory to remove the highly polluted and coloured wastewater in order to meet the legislative requirement and decrease the

seriousness of water pollution. Yet, some of them still failed to meet the discharge limits (Pang and Abdullah, 2013).

## **2.2 Textile effluents and regulation**

Textile industries have become a source of income for some countries, such as India and China. The increase demand of clothing and apparel has brought both positive consequences to some countries in a way, which is an improvement in economy, or in negative extreme attributed to environmental pollution. The untreated textile wastewater is high in color, chemical oxygen demand (COD), biochemical oxygen demand (BOD), total organic carbon (TOC), suspended solids (SS), pH, temperature, turbidity, and toxicity (Pang and Abdullah, 2013). Textile production required large quantity of chemical and fresh water in various processes (dyeing, finishing, sizing and rinsing) (Temesgen *et al.*, 2018).

In Malaysia, textile industry effluent discharges must comply with Environmental Quality Act 1974 and subsidiary legislation act, Environmental Quality (Industrial Effluent) Regulations 2009. Table 2.1 shows the acceptable conditions for discharge of industrial effluent or mixed effluent of standards A and B. The classification of standards A and B are based on the location of the industrial area, which is discharged upstream and downstream region of the water reservoir, respectively. Previously, the Hazen method is commonly used for the measurement of color unit which based on the concentration of platinum (Pt) in the hexachloroplatinate and cobalt ion (Co) in hydrochloride acid. However, the current color unit used in Malaysia is American Dye Manufacturers Institute (ADMI) color which based on the spectrophotometric method (Pang and Abdullah, 2013).

Table 2.1 Acceptable conditions for discharge of industrial effluent for mixed effluent of standards A and B (Department of Environment Malaysia, 2010)

Parameter	Unit	Standard	
		A	B
Temperature	°C	40	40
pH Value	-	6.0-9.0	5.5-9.0
BOD at 20 °C	mg/L	20	40
Suspended Solids	mg/L	50	100
Mercury	mg/L	0.005	0.05
Cadmium	mg/L	0.01	0.02
Chromium, Hexavalent	mg/L	0.05	0.05
Chromium, Trivalent	mg/L	0.20	1.0
Arsenic	mg/L	0.05	0.10
Cyanide	mg/L	0.05	0.10
Lead	mg/L	0.10	0.5
Copper	mg/L	0.20	1.0
Manganese	mg/L	0.20	1.0
Nickel	mg/L	0.20	1.0
Tin	mg/L	0.20	1.0
Zinc	mg/L	2.0	2.0
Boron	mg/L	1.0	4.0
Iron (Fe)	mg/L	1.0	5.0
Silver	mg/L	0.1	1.0
Aluminium	mg/L	10	15
Selenium	mg/L	0.02	0.5
Barium	mg/L	1.0	2.0
Fluoride	mg/L	2.0	5.0
Formaldehyde	mg/L	1.0	2.0
Phenol	mg/L	0.001	1.0
Free Chlorine	mg/L	1.0	2.0
Sulphide	mg/L	0.50	0.50
Oil and Grease	mg/L	1.0	10
Ammoniacal Nitrogen	mg/L	10	20
Colour	ADMI	100	200

### 2.3 Dyes removal techniques

In Malaysia, each textile industry factory treats its own wastewater and the treated effluents are normally discharged to a drain but not to a centralized treatment system (Pang and Abdullah, 2013). There are plentiful techniques to treat dye effluents. The treatments can be divided into three categories: chemical, biological and physical. All of these treatment have their own advantages and disadvantages as shown in Table 2.2.

Chemical treatment are methods utilizing chemistry or its theories in accomplishing dye removal. Conventional chemical treatments such as oxidative, ozonation, photochemical, and electrochemical destruction processes (Regti *et al.*, 2017). Most of these processes are expensive compared to biological and physical techniques and commercially unattractive because involves high electrical energy. High electrical energy is required to power equipment or reactors in which chemical dye removal takes place. Furthermore, chemical as well as reagent consumption on a large scale results in secondary pollution that eventually led to additional disposal problem (Katheresan *et al.*, 2018).

The biological treatment is commonly utilized for dye wastewater treatment in most countries. It is incorporates living organism such as fungi (especially white-rot), bacteria, yeasts and algae (Boudechiche *et al.*, 2016). The use of enzymes for dye removal from water is a favourite nowadays as it is believed to be the cheapest and safe technique. However, since this technique deals with living things, its main drawback is its growth rate. Instability of the process is common in biological dye removal processes as predicting its growth rate and reactions can be complicated at times (Katheresan *et al.*, 2018).



Table 2.2 Advantages and disadvantages of dye removal methods

Methods	Advantages	Disadvantages	References
<b>Chemical treatments</b>			(Dawood and Sen, 2014; Uday <i>et al.</i> , 2017)
Oxidative process	Simplicity of application	(H <sub>2</sub> O) agent needs to be activated by some means	
Ozonation	Ozone can be applied in its gaseous state and does not increase the volume of wastewater and sludge	Short half-life (20 min)	
Photochemical	No sludge is produced and foul odours are greatly reduced	Formation of by-products	
Electrochemical destruction	No consumption of chemicals and no sludge buildup	Relatively high flow rates cause a direct decrease in dye removal	
<b>Biological treatments</b>			(Jeanmonod <i>et al.</i> , 2018; Katheresan <i>et al.</i> , 2018)
Decolourisation by white-rot fungi	White-rot fungi are able to degrade dyes using enzymes	Enzyme production has also been shown to be unreliable	
Anaerobic textile dye bioremediation systems	Allows azo and other water-soluble dyes to be decolourised	Anaerobic breakdown yields methane and hydrogen sulphide	
<b>Physical treatments</b>			(Salleh <i>et al.</i> , 2011; Yagub <i>et al.</i> , 2014)
Adsorption by activated carbon	Good removal of wide variety of dyes	Commercially available AC are non-renewables and polluting precursor such as coal.	
Membrane filtration	Removes all dye types	Concentrated sludge production	
Ion exchange	Regeneration: no adsorbent loss	Not effective for all dyes	
Electrokinetic coagulation	Economically feasible	High sludge production	

Physical treatment are usually straightforward techniques normally accomplished by the mass transfer mechanism. Conventional physical dye removal methods are adsorption, membrane filtration, ion exchange and electrokinetic coagulation. Electrokinetic coagulation technique uses a direct current source between metal electrodes such as aluminium and iron immersed in water effluent to cause the dissolution of metal plates into wastewater (Dawood and Sen, 2014). The optimum coagulant concentration depends on the static charge of the dye solution, and the difficulty in removing the sludge formed as part of the problem with this method (Sharma, 2015).

Among all methods, adsorption process is the most commonly and preferred technique of dye removal due to its outstanding ability to remove almost any type of dyestuff which discussed in detail in the next section.

## **2.4 Adsorption**

The term adsorption refers to the accumulation of a substance at the interface between two phases either liquid–solid interface or gas–solid interface. Adsorbate referring to the substance that accumulates at the interface while adsorbent is define as the solid on which adsorption occurs. Adsorption process broadly used due to its flexibility and simplicity of design, low cost, insensitivity to toxic contaminants and ease of operation, to eliminate certain classes of chemical pollutants from waters. This process provides an attractive alternative for the treatment of polluted water, especially if the sorbent is cheap and does not require an additional pre-treatment step before its application. There are so many factors that affect the adsorption efficiency include adsorbate–adsorbent interaction, adsorbent surface area, adsorbent to adsorbate ratio, adsorbent particle size, temperature, pH and contact time (Yagub *et al.*, 2014).

Adsorption can be categorized into chemical sorption (chemisorption) and physical sorption (physisorption) as shown in Table 2.3.

Chemisorption is an irreversible sorption process due to formation of strong chemical interaction between molecules or ions of adsorbate to adsorbent surface which commonly involves the exchange of electrons (Sun *et al.*, 2016). On the other hand, physisorption is characterized by weak Van der Waals bonds between adsorbate and adsorbent and thus reversible in most cases (Katheresan *et al.*, 2018). The main physical forces controlling adsorption are Van der Waals forces, hydrogen bonds, polarity and dipole–dipole  $\pi$ – $\pi$  interaction (Ali, 2010).

Table 2.3 Comparison of physisorption and chemisorption

Criteria	Physisorption	Chemisorption	Reference
Bonding force	Van der Waal's forces	Chemical bond forces	(Yagub <i>et al.</i> , 2014)
Reversibility	Reversible	Irreversible	(Gisi <i>et al.</i> , 2016)
Chemical change of adsorptive	No new compound is formed in the process	New compounds are formed at the surface of adsorbent	(Králík, 2014)
Specificity of adsorbate-adsorbent interactions	Not very specific	Highly specific	(Králík, 2014)
Activation energy	Low activation energy 5 and 40 kJ/mol	High activation energy 40 to 800 kJ/mol	(Ahmed and Theydan, 2013)

## 2.5 Activated carbon

AC is a carbon-rich materials which contain well-built internal pore structure and become an ideal AC with characteristic of high surface area and a wide range of

chemical functional groups present on the surface which can make it more versatile with numerous applications (Danish and Ahmad, 2018). Any material containing high levels of carbon can be derived as AC. Apart from dye effluent, AC is capable of removing a number of pollutants present in wastewater such as heavy metals, detergents, herbicides, pesticides and polyaromatic hydrocarbons. AC prepared from different raw materials will have different adsorption capacities, surface area, pore structure, surface charge and surface chemistry (Peng *et al.*, 2018a).

### **2.5.1 Source of AC**

Commercially available AC produced from bituminous coal and coke are considered costly and nonrenewable, therefore there are growing research interest in exploring alternative renewable, widely available and economical precursors (Basta *et al.*, 2019). ACs have been prepared from other alternative resources such as date stones (Abbas and Ahmed, 2016), coconut shells (Mohammed *et al.*, 2015), pomegranate peel (Ahmad *et al.*, 2014), oil palm shells (Hesas *et al.*, 2013a), peanut shells (Georgin *et al.*, 2016), coffee shells (Li *et al.*, 2016a), palm kernel shells (Kundu *et al.*, 2015a), Jatropha (Khalil *et al.*, 2013), rice husks (Muniandy *et al.*, 2014), hazelnut husk (Karaçetin *et al.*, 2014), pineapple peels (Foo and Hameed, 2012b), peanut hulls (Silva *et al.*, 2017), cocoa bean husk (Plaza-Recobert *et al.*, 2017), cashew nut shell (Subramaniam and Ponnusamy, 2015; Spagnoli *et al.*, 2017), orange peel (Lam *et al.*, 2017) and palm kernel shell (García *et al.*, 2018).

### **2.5.2 Wood residues as a precursor**

The wood industry has become a major source of foreign exchange across the globe. Due to this, wood wastes represent wastes that are to be disposed of as a secondary resource to be exploited. In addition, most of the wood plants are being built

up in developing countries such as Malaysia, Nigeria, and Indonesia, which are active in forest development (Shafie *et al.*, 2017). Mass quantity of wood waste is generated from by-products of wood-related activities such as saw and plywood milling. Saw milling residues comprises of sawdust, off cuts, slabs, shavings, and bark, meanwhile in plywood mills residues generated in the form of veneer cores, defective ends and irregular pieces of veneer sheets (Osman *et al.*, 2014). Sawdust materials are biodegradable and can be used as a low-cost adsorbent due to its lignocellulosic composition. It comprises abundant lignin, cellulose, hemicellulose and some functional groups such as hydroxyl, carboxyl, amide and phenolic groups in its structure, which make the adsorption processes possible (Sahmoune and Yeddou, 2016). On an average, the quantitative proportion of hemicellulose, cellulose, and lignin in wood biomass are observed in the range of 20–35, 40–50, and 15–35 %, respectively (Danish and Ahmad, 2018).

There are few studies use sawdust as a precursor for AC production. AC was derived from *Tectona Grandis* tree using physical activation with carbon dioxide and exhibit higher surface area of 910 m<sup>2</sup>/g (Cansado *et al.*, 2018). Kazemi *et al.* (2016) synthesize AC from fir wood sawdust and found that the surface area of the prepared AC enhanced from 1273 m<sup>2</sup>/g to 1789 m<sup>2</sup>/g along with an increase in the IR of H<sub>3</sub>PO<sub>4</sub> from 1 to 1.5. On the other hand, pine sawdust based AC produced low surface areas below 400 m<sup>2</sup>/g by modification of the precursor with a calcium chloride solution before the carbonization process (Aguayo-Villarreal *et al.*, 2016).

In this study, an attempt was made in using sawdust from PS, IS and HS species obtained from local wooden furniture manufacturing. *Pentace triptera* (PS) wood is a genus of wood species in the *Tiliaceae* family which can be found in Malaysian forest and other ASEAN countries. The timber is 40 m tall light hardwood

with a density of 530-755 kg/m<sup>3</sup> air dry. The timber is suitable for light construction, finishes, panels, furniture, flooring, boat construction, interior decoration and plywood making (Farrokhpayam *et al.*, 2010).

*Intsia bijuga* (IS) wood belongs to family of *Fabaceae* widely distributed from Madagascar towards Malaysia, Indonesia, Australia and Polynesia (Nugroho *et al.*, 2010). It is classified as a good quality that yield attractive dense wood and is one of the most valuable woods which is highly prized (Marler, 2016). The timber is a heavy hardwood with 42-50 m and density of 515-1,040 kg/m<sup>3</sup> air dry. IS is commercially used in flooring, doors and panels and in marine equipment (Keong, 2006).

*Hevea brasiliensis* (HS) is one of the most ecological wood species because mainly grown for its latex and cut down when it becomes unproductive (Kumar *et al.*, 2005). About 80 % of the world's rubber plantations are based in southeast Asia where Malaysia and Thailand are the world's highest producers of rubber (Shigematsu *et al.*, 2011). It is a light hardwood with a density of 560 - 640 kg/m<sup>3</sup> air dry. It has become one of the main wood for the manufacture of furniture and interior building components such as wood panel, chip board, cement-bound board, medium-sized fiberboard and furniture (Junior *et al.*, 2015).

### **2.5.3 Classification of porous materials**

An ideal AC should possess characteristics such as a high surface area and well developed pores. According to the International Union of Pure and Applied Chemistry (IUPAC) (Burwell, 1976), the pores on AC surface can be classified into three types (Figure 2.1):

- (i) Micro pores type (pore size  $< 2$  nm).
- (ii) Meso pores type (pore size 2-50 nm).
- (iii) Macro pores type (pore size  $> 50$  nm).

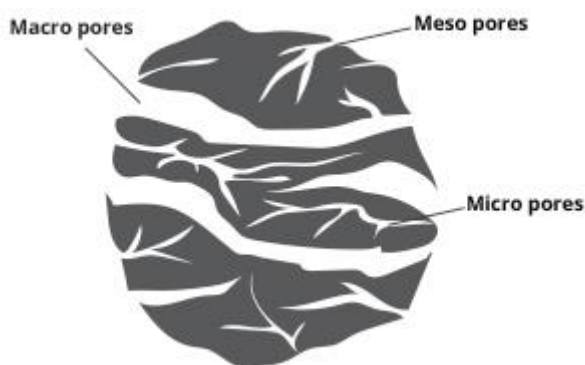


Figure 2.1 Porous structure of AC (Suresh Kumar *et al.*, 2017)

Nitrogen adsorption-desorption isotherm studies were usually conducted to quantifying porosity of AC produced. Figure 2.2 illustrate six types (Type I-VI) of the adsorption isotherm based on the plot trend. For Type I, the plot increases rapidly at low relative pressures ( $P/P_0$ ) and it slows down at moderate pressure, thus, revealing the micropore and mesopore structure. At low relative pressures, the adsorbance of Type II adsorption isotherm sharply increases, representing the existence of micropore filling. The Type III adsorption isotherm is convex to  $P/P_0$  axis which displays the weak interaction of adsorbent and adsorbate.

The hysteresis loop of Type IV reflects the connectivity of various sized pores and the adsorbent develops considerable micropore and mesopore. The Type V adsorption isotherm increases slowly at the low relative pressure showing poorly developed micropore, then it sharply rises revealing large numbers of mesopores development. The Type VI isotherm, in which the sharpness of the steps depends on

the system and the temperature, represents stepwise multilayer adsorption on a uniform non-porous surface (Zhang *et al.*, 2016).

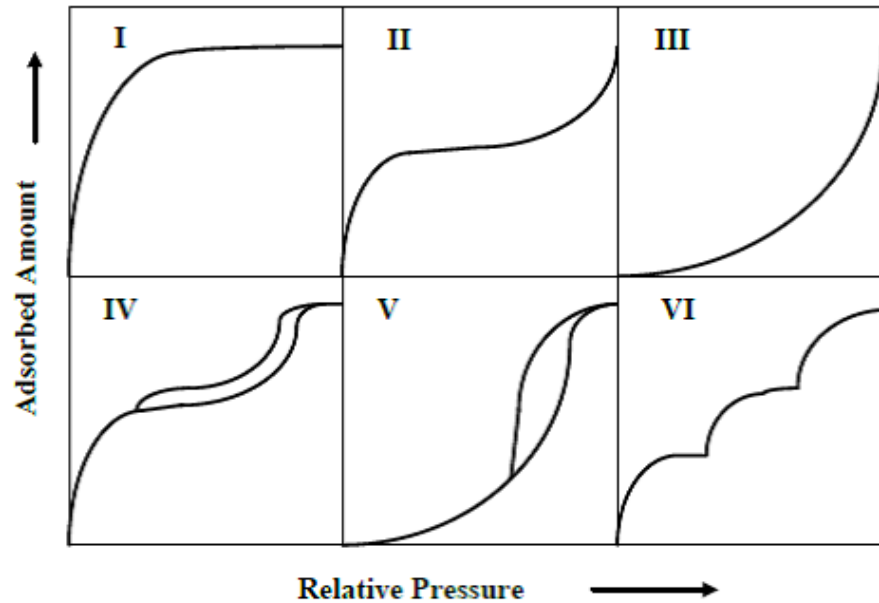


Figure 2.2 Type of adsorption isotherm (Zhang *et al.*, 2016).

The hysteresis loop can be connected with four pore types namely H1, H2, H3 and H4 as shown in Figure 2.3. H1 hysteresis loop featured by a strait loop, indicates a limited pore size distribution of the measured samples, and the adsorption and desorption branch is parallel to each other and perpendicular to the axis of pressure in a wide pressure range. There is an inflection point for H2 for a sudden drop of desorption branch, which is associated with bottle neck pores (Zhang *et al.*, 2016). The extreme adsorption and desorption branch of H3 does not appear for it usually occurs with open-wedge pores. The hysteresis loop of H4 is wide and the desorption curve is steeper than adsorption branch, showing that the samples have various distributions of pore types and pore diameter, which usually happens to slit-like pores and two parallel-plate cracks.



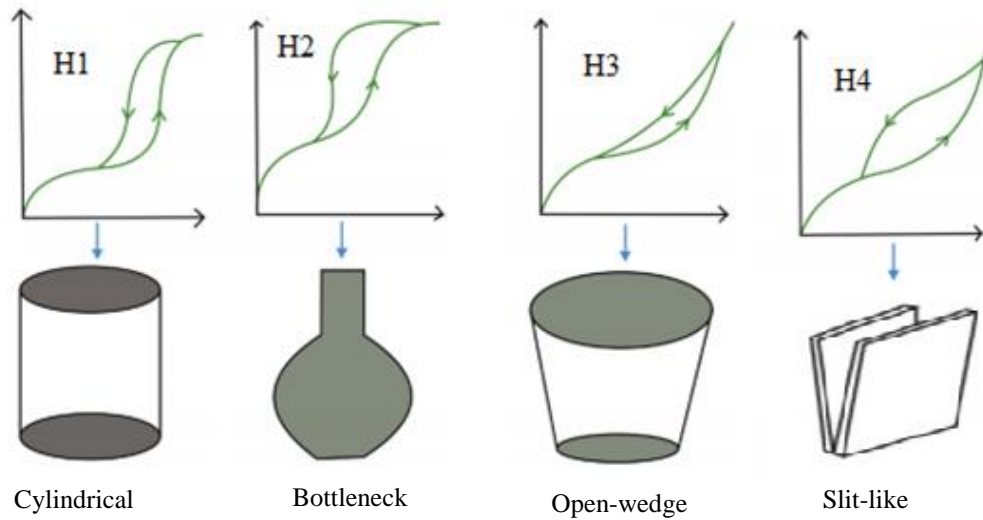


Figure 2.3 Classification of hysteresis loops and their related pore shapes (Zhang *et al.*, 2016)

## 2.6 Production of AC

Carbonization and activation step are two important steps in the production of AC. The first step is to enrich the carbon content and to create an initial porosity and the activation process helps in enhancing the pore structure. Activation is commonly performed via conventional heating sources such as electrical oven or furnace but recently, many researchers have been switching into microwave irradiation technique due to several advantages that it offers (Lam *et al.*, 2017).

### 2.6.1 Carbonization process

Carbonization is conducted at temperature of 100 – 600 °C in the inert environment (using N<sub>2</sub> gaseous) for char formation (Olivares-Marín *et al.*, 2012). Based on temperature variation, the carbonization process can be categorized into four main steps as summarized in Table 2.4. This process enriches the carbon content from the organic substances and create initial pores on the surface. However, the pores formed during the carbonization process are typically narrow. The pores formed when volatile constituents from the carbon matrix diffuse out leaving the sample in gas

phase. Some substances may collide with the walls of the pores, resulting in hydrocracking and carbon deposition (Chowdhury *et al.*, 2013).

Table 2.4 Steps and range of temperature in the carbonization process (Chowdhury *et al.*, 2013)

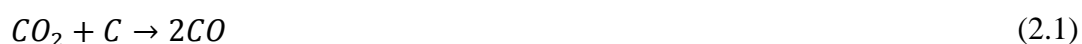
Stages	Temperature (°C)	Process
1	$T \leq 200$	Initial drying of precursor to remove its moisture content.
2	$200 \leq T \leq 400$	Small quantities of non-condensable gas such as CO and CO <sub>2</sub> can be obtained.
3	$400 \leq T \leq 500$	Bulk of the light tar produced released as volatile gas.
4	$500 \leq T \leq 600$	Remaining volatile component is driven away resulted in an increase in carbon percentage of char.

## 2.6.2 Activation process

In the activation step, the carbonized material is subjected to secondary reactions to increase its surface area as well as enhance the pore structure (Chen *et al.*, 2018). The textural properties of adsorbents usually changed after undergoing activation process. In addition to the textural properties, the surface chemistry strongly affects the adsorption capacity of ACs (Chowdhury *et al.*, 2013). There are three main methods for activation, namely physical, chemical and physicochemical processes.

### 2.6.2 (a) Physical activation

Physical activation is conducted using oxidizing gas such as CO<sub>2</sub>, steam, air or their mixtures at 700 to 1000 °C (Tan *et al.*, 2017). The following reaction takes place between CO<sub>2</sub> and the carbon matrix:



Steam and air have been shown to react 8 times and 100 times faster respectively with carbon than CO<sub>2</sub> and therefore caused uncontrollable reaction (Chowdhury *et al.*, 2013). Steam and air react with carbon elements to produce CO and CO<sub>2</sub> by the following reactions:



The aggressive reaction of air caused by O<sub>2</sub> with carbon had caused excessive burning in the inner pores and the outer surface of the carbon which results in excessive weight loss. Furthermore, another advantage on using CO<sub>2</sub> as activating gas as it is easy to handle and clean, and ensures overall control of the activation process due to the slow reaction rate at temperatures around 800 °C (Menya *et al.*, 2017).

### 2.6.2 (b) Chemical activation

Chemical activation technique involves the impregnation of the material with a dehydrating chemical agent such as sulphuric acid (H<sub>2</sub>SO<sub>4</sub>), nitric acid (HNO<sub>3</sub>), phosphoric acid (H<sub>3</sub>PO<sub>4</sub>), zinc chloride (ZnCl<sub>2</sub>), potassium hydroxide (KOH), sodium hydroxide (NaOH), calcium carbonate (K<sub>2</sub>CO<sub>3</sub>) (Ahmad *et al.*, 2012; Kamandari *et al.*, 2015; Rashidi and Yusup, 2017). The chemical agents help to develop the pores in the AC using degradation, dehydration and complexation with organic carbon molecules of precursor materials (Danish and Ahmad, 2018).

Typically, chemical activation is performed at lower temperatures than physical activation because chemical interactions between the remaining chemicals of

biomass and activating agents offset this temperature gap and thus helps in saving energy. The other major advantages are higher yield, save time, incorporation of suitable functional groups, and larger surface area of the AC. The major disadvantage of this process is the cost of chemicals and involve an additional process of flushing AC with hot and cold water to remove the left-over unreacted chemicals. Furthermore, there are some environmental concerns by using chemical agents during the activation process, therefore the selection of the right chemical agent and harmless to the environment is an important factor (Chowdhury *et al.*, 2013).

### **2.6.2 (c) Physicochemical activation**

AC can also be produced through physicochemical activation which combined physical and chemical activation process. This process involve the sample impregnation with chemical agent followed by heat treatment in the presence of oxidizing gas at 200-900 °C (Chowdhury *et al.*, 2013). The combination of chemical and physical activation contributes to the development of the pores textural and chemical characteristics compared to single activation method. Physicochemical activation is conducted when chemical agent is not fully diffused and thus results in pore clogging. Consequently, gasification is needed in the presence of steam or CO<sub>2</sub> during the activation (Rashidi and Yusup, 2017).

### **2.7 Microwave heating activation**

During activation process, thermal heating is conducted using an electric furnace as a conventional way where the energy is transferred from an outer surface to the inner through conduction and convection. The thermal gradient causes a prolonged time in achieving the desired activation temperature which resulted in the formation of ashes (Hesas *et al.*, 2013b). Furthermore, the heating do not happen uniformly due